Available online at www.sciencedirect.com

ScienceDirect

Procedia CIRP 141 (2026) 43–48

www.elsevier.com/locate/procedia

10th Conference on High Performance Cutting (CIRP-HPC 2026)

Multi-Sensor Analysis of Tool Wear with Integration of Direct and Indirect Sensors

Ehsan Karimi[a,*], Jannik Schwalm[a], Volker Schulze[a]

[a]*wbk Institute of Production Science, Karlsruhe Institute of Technology (KIT), Kaiserstr. 12, 76131 Karlsruhe, Germany*

* Corresponding author. Tel.: +49-1523-9502572; fax: +49-721-608-45004. *E-mail address:* ehsan.karimi@kit.edu

Abstract

Accurate analysis of tool wear is essential for the efficient tool utilization, enhancing productivity and minimizing machine downtime. Direct sensors, such as optical vision systems, provide precise measurements but are sensitive to alignment and environmental conditions. Indirect sensors, including cutting force and acoustic emission, offer complementary process information and can be integrated into machining environments for real-time monitoring. However, their signals are often unstable and strongly affected by vibration noise, limiting the performance of conventional signal-processing techniques. This study introduces a multi-sensor framework that combines direct and indirect measurements in an image-based workflow for tool wear characterization. Images of the cutting edge, captured by a camera, are processed with a U-Net segmentation model to analyse the wear. In parallel, cutting force and acoustic emission signals are transformed into image-based representations using Gramian Angular Field (GAF) mapping. Together, these data sources enable a unified approach to tool wear analysis. Deep convolutional neural network method is employed to extract discriminative features and improve robustness against measurement uncertainties. While optical measurements provide precise wear characterization, they are difficult to integrate for continuous on-machine monitoring due to alignment sensitivity and time requirements. In contrast, indirect sensors can be seamlessly integrated into the machining environment. Experiments on milling processes show that GAF-based signal representations allow indirect sensors to operate more independently of optical monitoring while enabling in-process tool wear analysis in the presence of vibration disturbances. The proposed method supports real-time, on-machine condition monitoring and contributes to the development of intelligent manufacturing.

Peer-review under responsibility of the scientific committee of the 10th Conference on High Performance Cutting (CIRP-HPC 2026)

Keywords: Wear; Condition monitoring; Artificial intelligence

1. Introduction

In modern manufacturing, ongoing advancements in digitalisation and intelligent production are driving efforts to improve efficiency, stabilise processes and enhance product quality. As production systems become more automated and data-driven, it is essential to continuously monitor and optimize machining operations to ensure reliability. Cutting tools play a critical role in machining processes as the final elements interacting with the workpiece [1,2]. The progression of tool wear directly affects surface integrity, dimensional accuracy, machining efficiency, and production cost [3]. Excessive wear can lead to reduced product quality, unstable cutting conditions, or even tool failure, which may cause machine downtime and scrap production. Therefore, the development of effective tool condition monitoring (TCM) and prediction of tool wear are essential for ensuring reliable machining performance and increasing processing efficiency [4]. In modern machining environments, TCM approaches are generally categorized into two main groups: direct and indirect monitoring methods [5,6]. Direct monitoring techniques, such as optical inspection, laser-based measurement tool and resistance measurements, aim to evaluate the condition of the tool by directly observing wear or edge degradation. While these methods can provide highly accurate wear information, they often necessitate interrupting the machining process, thereby reducing production efficiency. Their performance

2212-8271
Peer-review under responsibility of the scientific committee of the 10th Conference on High Performance Cutting (CIRP-HPC 2026)
10.1016/j.procir.2026.03.111

can also be affected by factors such as chip accumulation, coolant flow and limited accessibility to the cutting area [7].

In contrast, the second category comprises indirect sensor-based monitoring approaches that infer tool wear by analyzing measured process signals rather than by directly observing the tool surface. These techniques rely on sensor data, such as cutting forces, vibration or acoustic emission signals, acquired directly from the machine tool during operation [6]. Unlike direct methods, indirect approaches enable continuous, real-time monitoring without halting the machining process, making them more suitable for industrial applications [8]. However, indirect monitoring remains sensitive to environmental noise, machine tool dynamics and varying process conditions, which can reduce its robustness and accuracy. Therefore, selecting an appropriate monitoring strategy is essential to ensure reliable performance across diverse manufacturing environments.

To effectively analyze these indirect sensor signals, time–frequency transformation, such as continuous wavelet transforms (CWT) and image-encoding techniques have gained increasing attention in recent years. Among them, the gramian angular field (GAF) has emerged as a powerful method for converting one-dimensional time-series data such as vibration, force, or acoustic emission signals into two-dimensional images while preserving both temporal structure and global correlations within the signal [9]. GAF not only retains the original information of the waveform, but also encodes pairwise relationships between all sampling points, thereby enriching the representation of fault-related patterns compared with raw signals. As demonstrated in several studies [2,10,11] GAF-encoded images significantly enhance feature separability and improve diagnostic performance when combined with convolutional neural networks. This capability makes GAF particularly suitable for tool condition monitoring, where subtle variations in process signals must be captured reliably under varying machining conditions [12].

In summary, extensive developments have been made in both direct and indirect TCM approaches. However, these methods are often used in isolation, meaning their complementary strengths are not fully exploited [13]. In this study, our aim is to integrate these two monitoring strategies into a multi-sensor framework, using direct measurements to train and validate indirect, signal-based models. This combined approach enables on-machine, in-process monitoring and prediction of tool wear.

2. Material and Methods

2.1. Experimental setup

The experiments were conducted on a 3-axis milling machine (POS CE10001) using a C45 steel workpiece with a 100 × 100 mm² cross-section and a machining length of 150 mm. Milling tests were performed at cutting speeds v_c = 133 and 86 m/min. Down-milling was carried out with feed per tooth f_z = 0.015, 0.025, and 0.050 mm/tooth. The cutting parameters were adjusted based on the tool diameter. For the 5 mm end mill, the cutting width and depth were set to a_e = 1.5 mm and a_p = 2.5 mm. For the 8 mm end mill, cutting width was increased to a_e = 4 mm while cutting depth remained at a_p = 2.5 mm. Both tools were four-flute HOLEX Pro Steel end mills made of cemented carbide with a TiAlN coating. Compressed air was supplied through a nozzle to remove chips from the tool and workpiece surface during machining.

2.2. Multi-sensor measurement system

As direct sensor a smart camera (Baumer VAX-50 M.I.NVX) was installed on the milling machine to capture high-resolution images of the cutting tool. The system integrates a 5-megapixel monochrome sensor with a resolution of 2448 × 2048 pixels and an NVIDIA Jetson Xavier NX module for on-board execution of AI algorithms. The camera is combined with a video microscope unit (Mitutoyo VMU-V) and a Mitutoyo M Plan Apo 2X objective lens to ensure precise imaging of the cutting edges. Images were recorded every five machining passes along the 150 mm cutting path, covering all four cutting edges of the tool. A 24 V trigger signal from the milling machine initiated each image capture. After each set of five passes, the tool was automatically moved to the correct working distance of the objective lens, and images of all four cutting edges were acquired by rotating the tool to a defined angular position.

Two different indirect sensors were used to collect the process signals. Cutting forces were measured using a Kistler triple-component piezoelectric dynamometer (Type 9255C) equipped with a charge amplifier and operated at a sampling rate of 10 kHz. The 10 kHz sampling rate was selected to exceed the dominant tooth-passing frequency; for a spindle speed of approximately 8500 rpm and a four-flute tool, the resulting tooth-passing frequency is about 568 Hz, with harmonics below 3 kHz, ensuring accurate acquisition of the relevant force dynamics without distortion. The dynamometer assembly was rigidly mounted between the workpiece and the machine table to ensure stable force transmission. In addition to force measurement, acoustic emission (AE) signals were acquired using a Kistler Piezotron AE sensor (Type 8152C), designed for high-frequency monitoring in the 50–400 kHz range. The AE sensor was mounted directly on the workpiece using a M6 screw, ensuring reliable coupling of high-frequency elastic waves. The sensor output was conditioned using a Kistler Piezotron AE coupler (Type 5125C), which provided signal amplification, integrated RMS conversion, and band-pass filtering using a 50 kHz high-pass and a 1 MHz low-pass stage before transmission to the data acquisition system. The schematic setup is shown in Figure 1.

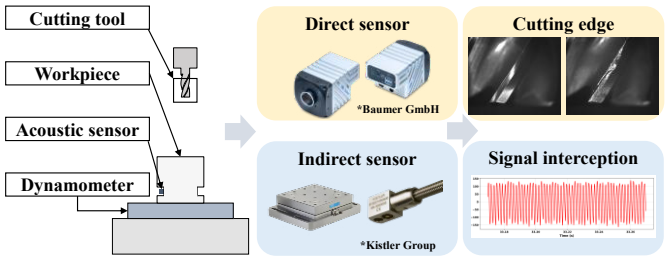

Fig. 1. Experimental setup.

2.3. Image processing and wear measurement (Direct sensor)

The images collected by the integrated camera in the milling machine were processed following the workflow established in our previous on-machine wear analysis study, which combines a semantic segmentation model with computer vision techniques [13]. A U-Net-based supervised segmentation model, trained on manually labeled flank-wear masks (228 original images) and an augmented dataset (912 augmented images), was employed to automatically detect the flank wear area. This approach provides a robust binary mask of the worn region ensuring reliable extraction of wear characterization. To improve segmentation accuracy, images were first aligned using the enhanced correlation coefficient (ECC) algorithm, which maximizes similarity with a reference frame and compensates for small orientation variations. A fixed region of interests (ROI) of 1400 × 1000 px was then extracted to isolate the cutting edge and remove irrelevant background.

Following segmentation, maximum flank-wear width VB_{max} was calculated using a geometric measurement pipeline. Canny edge detection was applied to the binary mask to extract the wear boundary, and the largest contour was identified and enclosed in a minimum-area bounding rectangle. VB_{max} was obtained from the orthogonal distance between the rectangle's opposing edges. Measurements were performed every five passes, matching the image acquisition rate, enabling continuous monitoring of wear progression. The resulting wear values served as ground-truth labels for the indirect sensor signals and supported subsequent multi-sensor fusion and model training. Figure 2 illustrates the direct sensor workflow.

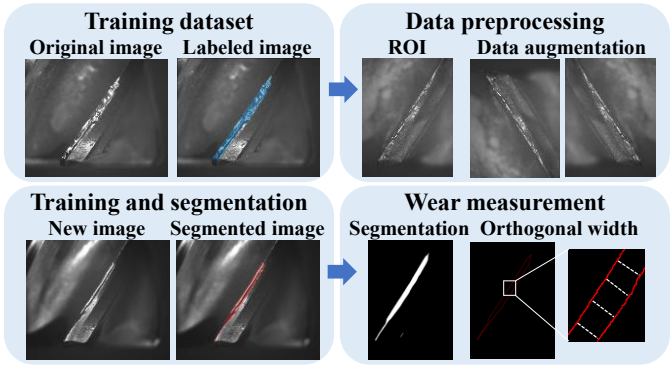

Fig. 2. Camera-based wear analysis of the cutting tool.

A hybrid data-filtering procedure was applied to improve the reliability of the wear measurements without discarding useful data. Density-based spatial clustering of applications with noise (DBSCAN) was first used to identify outlier values caused by misalignment, illumination changes, or residual chips. Instead of removing these points, locally weighted scatterplot smoothing (LOWESS) was used to estimate the expected wear at the corresponding cut positions, and each DBSCAN outlier was replaced with its LOWESS value. This combined approach effectively eliminated unrealistic measurement spikes while maintaining a continuous and physically meaningful wear curve for subsequent analysis.

2.4. Signal processing

Before applying GAF encoding, the acoustic emission and cutting-force signals were segmented and clustered to isolate the target cutting section. As outlined in Section 2.2, images were acquired every five passes, giving five corresponding sets of force and AE data per acquisition step. Although the axial force component F_z was recorded, it was not included in the subsequent analysis, as it showed no significant wear-related variation over the tool life and was more influenced by axial preload and structural effects. Each pass consists of three zones: a 10 mm entry, a 130 mm target cutting region, and a 10 mm exit, with the entry and exit performed at reduced speed (v_c = 12 m/min) to minimize vibration. As shown in Figure 3, segmentation produced 15 signal segments per cycle (5 passes × 3 zones). Only the target cutting region was used for further analysis, so the first processing step was to automatically identify and extract this segment from each pass.

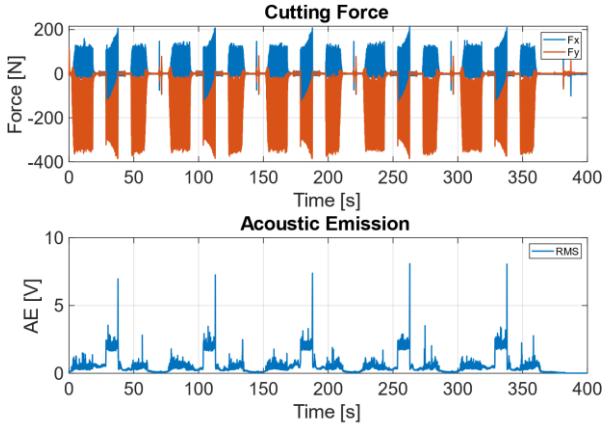

Fig. 3. Cutting forces and acoustic emission signals during machining.

Afterwards, a 0.1 s segment from each target section was extracted from both the force and acoustic emission signals and used for GAF analysis. The GAF is then constructed in the following steps [2,11]:

1. Piecewise aggregate approximation (PAA)

Given a time series $Z = \{x_1, \dots, x_T\}$, the signal is optionally reduced in length using piecewise aggregate approximation (PAA). In this procedure, the time series is divided into non-overlapping segments of equal length, and each segment is replaced by its mean value. This produces a shorter, smoothed representation.

$$\bar{Z} = \{\bar{x}_1, \dots, \bar{x}_N\} \qquad N \leq T \tag{1}$$

2. Min–max normalization to [0,1]

Each sample is first rescaled to the interval [0,1] to ensure a valid mapping to angular coordinates:

$$\tilde{x}_i = \frac{x_i - \min(\bar{X})}{\max(\bar{X}) - \min(\bar{X})} \qquad i = 1, \dots, N \tag{2}$$

3. Mapping to polar coordinates

The normalized value x_i is interpreted as the cosine of an angle, and the (normalized) time index as the radius:

$$\emptyset_i = \arccos(\tilde{x}_i), \; r_i = \frac{t_i}{N} \tag{3}$$

where t_i is the time index of sample i. In this way, $\emptyset_i$ preserves the signal magnitude information, while r_i encodes the temporal order of the samples.

4. Construction of the Gramian matrices

Using the polar angles, a Gramian matrix is formed by computing pairwise trigonometric combinations of all samples:

$$GASF_{ij} = \begin{bmatrix} \cos(\emptyset_1 + \emptyset_1) & \dots & \cos(\emptyset_1 + \emptyset_j) \\ \cos(\emptyset_2 + \emptyset_1) & \dots & \cos(\emptyset_2 + \emptyset_j) \\ \vdots & \ddots & \vdots \\ \cos(\emptyset_i + \emptyset_1) & \dots & \cos(\emptyset_i + \emptyset_j) \end{bmatrix} \quad (4)$$

$$GADF_{ij} = \begin{bmatrix} \sin(\emptyset_1 - \emptyset_1) & \dots & \sin(\emptyset_1 - \emptyset_j) \\ \sin(\emptyset_2 - \emptyset_1) & \dots & \sin(\emptyset_2 - \emptyset_j) \\ \vdots & \ddots & \vdots \\ \sin(\emptyset_i - \emptyset_1) & \dots & \sin(\emptyset_i - \emptyset_j) \end{bmatrix} \quad (5)$$

The resulting Gramian Angular Summation Field (GASF) and Gramian Angular Difference Field (GADF) encode both pointwise values and their temporal relationships in a two-dimensional structure, forming image-like representations suitable for neural-network–based tool-wear prediction. In this work, GASF matrices derived from force and acoustic-emission signals serve as inputs to the prediction model. An example is shown in Figure 4.

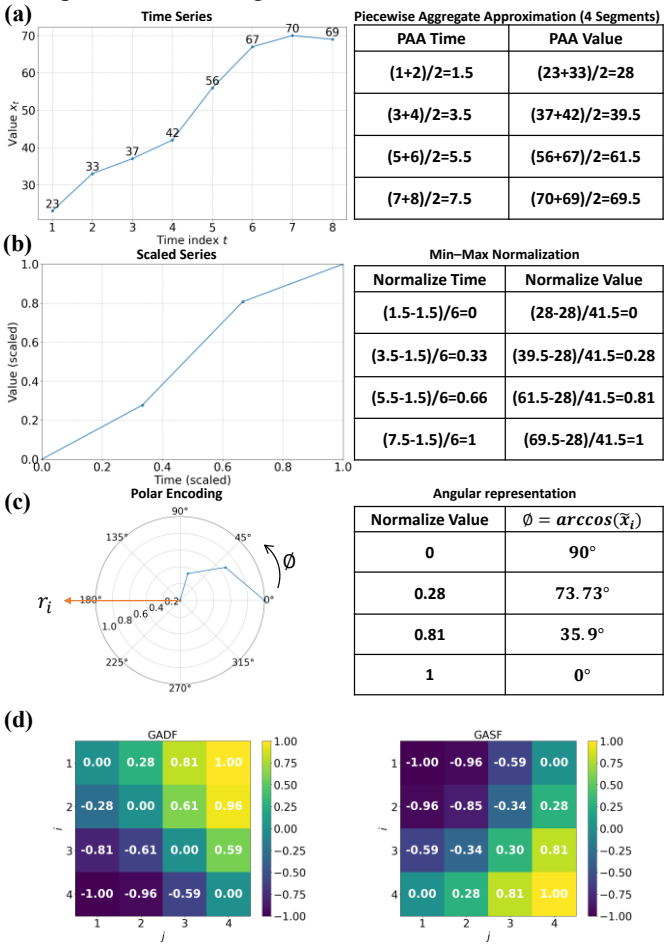

Fig. 4. Example workflow of generating a GAF image from a time-series signal. (a) Original time-series and PAA-reduced with 4 segments. (b) Normalized signal. (c) Mapping to polar coordinates. (d) Image representations of GADF and GASF matrices.

2.5. Deep learning workflow

The deep learning model was trained to predict tool wear range from indirect sensor data using the maximum flank-wear measurements obtained from the direct imaging system as ground-truth labels (Section 2.4). For each machining test, the minimum and maximum flank wear values over the full cutting length were computed from the image segmentation model and used to define a wear range $[VB_{min}, VB_{max}]$ for that test. This range reflects the progression of wear observed on the tool under the corresponding process conditions. For every GASF-encoded force and acoustic emission segment, the associated wear range of its test was assigned as the regression target. In this way, the indirect sensor signals learned to reproduce the wear behaviour quantified by the direct optical sensor. The dataset was built from four machining experiments covering early, mid, and late tool-life stages (S1–S3). GAF images were generated from the X- and Y-force signals and the RMS acoustic-emission signal without additional signal filtering, and machining parameters (v_c, v_f, f_z, d, a_e, a_p) were recorded inputs. Approximately 30% of samples from each experiment were selected, and an 80/20 stratified split ensured balanced wear-stage representation with no overlap between training and test data.

A multimodal CNN was developed to fuse GAF image features with machining parameters. The three GAF images passed through a shared convolutional backbone (four conv–pool blocks + global average pooling), while machining parameters were processed in a parallel fully connected branch. The fused features were fed into a regression head predicting $[VB_{min}, VB_{max}]$. Training used Adam (learning rate 10^{-3}, batch size 8), 400 epochs, and MSE loss; MAE was the main evaluation metric on the independent test set. All inference followed the same preprocessing steps. Figure 5 summarizes the workflow.

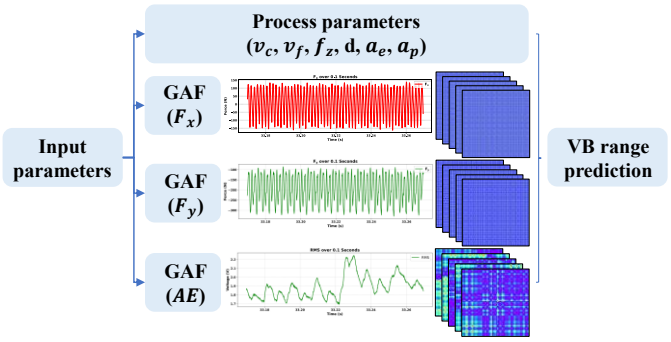

Fig. 5. Deep learning workflow.

3. Results

3.1. Optical wear analysis

After collecting images from the different tests, the trained segmentation model was applied to extract the flank-wear region and compute the corresponding VB_{max} value for each cutting-edge image, yielding wear-progression curves over the cutting length. Before using these curves as ground truth for the indirect sensor model, the raw wear data were filtered using a hybrid DBSCAN–LOWESS approach to remove segmentation artifacts while preserving the underlying wear trend. Each point on the filtered curve corresponds to one image acquisition step and represents the wear state associated with five consecutive passes, and thus with five

sets of force (F_X, F_Y) and acoustic-emission data (section 2.5). Figure 6 shows an example of a filtered wear curve exhibiting the expected monotonic increase with cutting length.

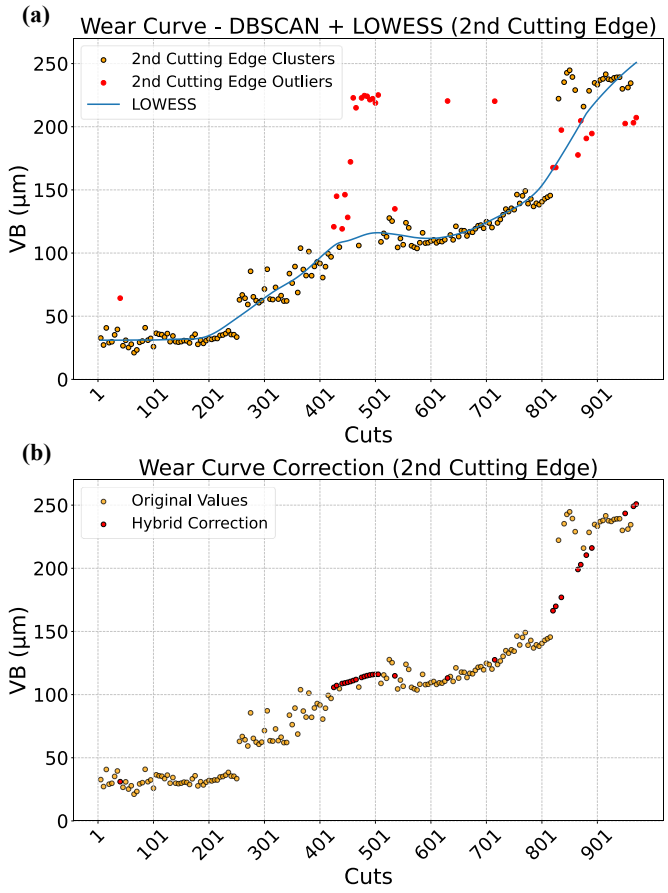

Fig. 6. Hybrid DBSCAN–LOWESS filtering applied to the wear progression. (a) Outlier detection and smoothed trend. (b) Corrected wear curve used as ground truth.

3.2. Signal-based analysis and GAF representation

Analysis of the segmented force signals revealed clear changes in the dynamic cutting behaviour as tool wear progressed. The extracted 0.1-s windows of signals showed increasingly irregular oscillations with higher wear, with early tool life characterised by smooth, periodic patterns and later stages exhibiting stronger fluctuations and higher-frequency components. These changes were clearly reflected in the Gramian Angular Summation Field (GASF) representations generated from the same segments. At low wear, the GAF matrices exhibited simple, uniform, and banded structures with well-defined symmetry, characteristic of stable and repeatable cutting forces. As wear increased, the matrices became progressively richer in detail, showing stronger contrast variations, more heterogeneous textures, and increasingly fragmented correlation patterns. This growing structural complexity mirrors the rise in temporal variability and irregularity observed in the force signals. Representative GAF images for low-, mid-, and high-wear conditions are shown in Figure 7, illustrating how the encoded force behaviour evolves from smooth and regular patterns to highly detailed and irregular structures as tool wear progresses.

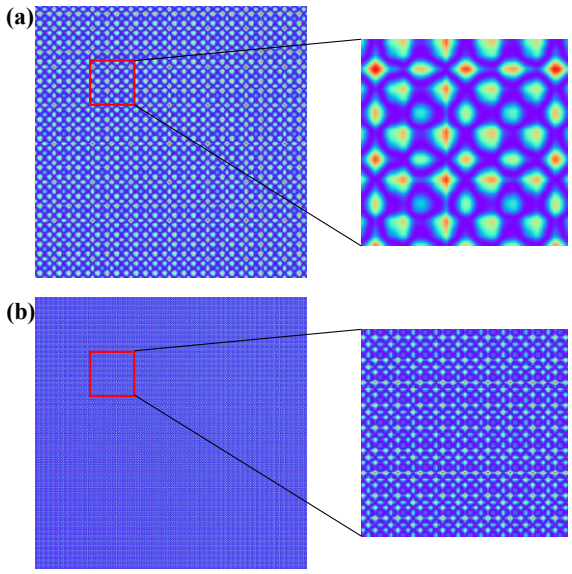

Fig. 7. Representative GAF images. (a) low-wear. (b) high-wear.

3.3. Deep learning model performance

The quality of the model predictions is illustrated in Figure 8, which compares the true wear ranges (shaded in orange) with the predicted wear intervals (shaded in green) along the sequence of cuts for v_c = 133 and 86 m/min and v_f = 1700 and 330 mm/min. The predicted wear envelopes follow the increasing wear trend with high fidelity and remain tightly aligned with the ground-truth intervals for most of the tool life. Small deviations appear only in isolated regions, typically where the directly measured VB curve exhibits residual noise or abrupt transitions. Overall, the overlap between the true and predicted intervals demonstrates that the indirect sensor model is able to estimate both the magnitude and progression of tool wear using only force-derived GAF images and machining parameters.

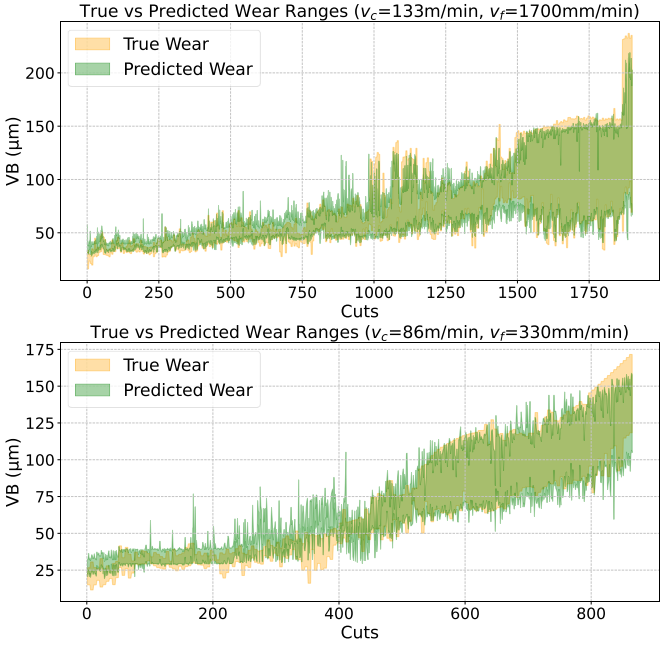

Fig. 8. True and predicted wear-range progression.

A quantitative evaluation was performed for both the lower and upper wear boundaries. For each sample, the absolute deviation between the predicted and true boundary values was computed, and predictions were considered correct when the error remained within a ±10 µm tolerance. Figure 9 provides the evaluation corresponding to the wear-range predictions shown in Figure 8. For the lower wear limit, the two evaluated cases yielded MAE values of 6.12 µm and 6.69 µm, with R^2 = 0.718 and 0.868. For the upper wear limit, the MAE values were 9.45 µm and 8.35 µm, with R^2 = 0.907 and 0.929. In both cases, the majority of samples fall within the ±10 µm tolerance band, indicating that the model reliably captures the evolution of the VB range and accurately reproduces both lower and upper boundary values.

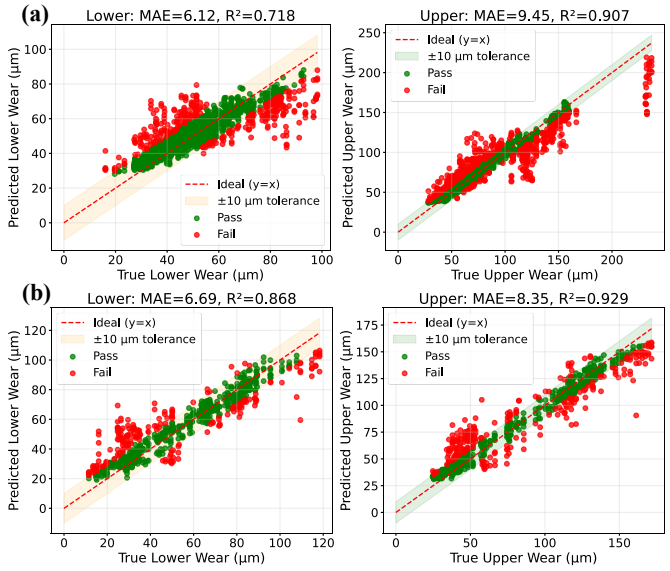

Fig. 9. True and predicted wear-range progression. (a) v_c = 133 m/min and v_f = 1700 mm/min (b) v_c = 86 m/min and v_f = 330 mm/min

4. Conclusion and outlook

The interval-based evaluation shows a clear difference in prediction performance between low and high wear levels. Using a dynamic threshold derived from the median true-midpoint wear (66.5 µm), the entire dataset from all tests was divided into a low-wear group (2135 samples with VB < 66.5 µm) and a high-wear group (2140 samples with VB ≥ 66.5 µm). Across all tests, the model consistently performed better in the high-wear region, while accuracy decreased at low wear values. This behaviour is clearly visible in the two-region scatter plots (Figure 10), where high-wear samples cluster near the ideal $y = x$ line, whereas low-wear samples show a broader spread.

These results align with the characteristics of the GAF-encoded force and acoustic-emission signals (Figure 7). As wear increases, the cutting process becomes more unstable, producing richer temporal patterns and stronger correlation structures in the GAF matrices, which provide the model with informative features. At low wear levels, however, signal changes are subtle and often fall within sensor and measurement noise, making early wear prediction inherently more difficult. From an application perspective, the stronger performance in the high-wear range is beneficial for preventing tool failure and planning timely replacement. Nevertheless, mispredictions also occur at the upper end of the wear range, indicating that the model still struggles to capture dynamics near maximum wear. While most mid-range predictions remain accurate, both the low-wear and extreme-high-wear intervals require further improvement. Future work will therefore focus on enriching the dataset with early-life and end-of-life samples, refining small-wear extraction, and exploring models that better capture subtle or nonlinear variations in the force and acoustic-emission signals.

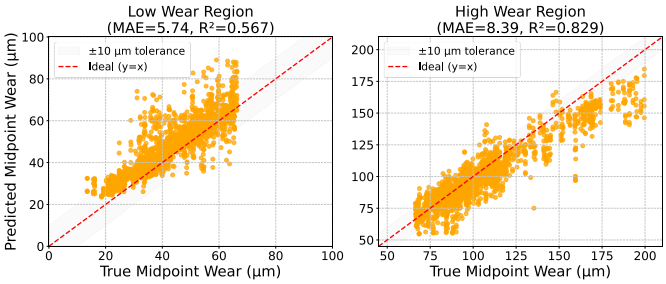

Fig. 10. True vs. predicted midpoint wear in low and high-wear regions.

Acknowledgements

This work was supported by the InnovationCampus Future Mobility, funded by the Ministry of Science, Research and the Arts of Baden-Württemberg under the Gaia-X4ICM project.

References

[1] Bergs T, Holst C, Gupta P, Augspurger T. Digital image processing with deep learning for automated cutting tool wear detection. Procedia Manufacturing 2020;48:947–58.
[2] Zhang Y, Qi X, Wang T, He Y. Tool Wear Condition Monitoring Method Based on Deep Learning with Force Signals. Sensors 2023;23:4595.
[3] Munaro R, Attanasio A, Del Prete A. Tool Wear Monitoring with Artificial Intelligence Methods: A Review. JMMP 2023;7:129.
[4] Denkena B, Wichmann M, Rokicki M, Stürenburg L. Modelling the influence of tool wear on shape errors in milling using a hybrid soft-sensor. Prod Eng Res Devel 2025;19:101–10.
[5] Kurada S, Bradley C. A review of machine vision sensors for tool condition monitoring. Computers in Industry 1997;34:55–72.
[6] Kuntoğlu M, Aslan A, Pimenov DY, Usca ÜA, Salur E, Gupta MK, et al. A Review of Indirect Tool Condition Monitoring Systems and Decision-Making Methods in Turning: Critical Analysis and Trends. Sensors 2020;21:108.
[7] Liu X, Yan H, Qiu L, Wang Y, Wang Z, Zhang Y, et al. Milling tool wear monitoring and forecasting with indirect multi-sensor information based on ResCNN and BiLSTM. J Mech Sci Technol 2025;39:6971.
[8] Hendricks S, Troß N, Brimmers J, Bergs T. Potential and challenges of tool condition monitoring in gear hobbing. Forsch Ingenieurwes 2022;86:807–18.
[9] Li G, Ao J, Hu J, Hu D, Liu Y, Huang Z. Dual-source gramian angular field method and its application on fault diagnosis of drilling pump fluid end. Expert Systems with Applications 2024;237:121521.
[10] Zhang Y, Shang L, Gao H, He Y, Xu X, Chen Y. A New Method for Diagnosing Motor Bearing Faults Based on Gramian Angular Field Image Coding and Improved CNN-ELM. IEEE Access 2023;11:11337.
[11] Cheng Y, Lu M, Gai X, Guan R, Zhou S, Xue J. Research on multi-signal milling tool wear prediction method based on GAF-ResNext. Robotics and Computer-Integrated Manufacturing 2024;85:102634.
[12] Hojati F, Azarhoushang B, Daneshi A, Hajyaghaee Khiabani R. Prediction of Machining Condition Using Time Series Imaging and Deep Learning in Slot Milling of Titanium Alloy. JMMP 2022;6:145.
[13] Karimi E, Schindler FA, Schulze V. On-Machine Flank Wear Analysis in Cutting Tools Using Artificial Intelligence. In: Drossel W-G, Ihlenfeldt S, Dix M, editors. Production at the Leading Edge of Technology, Cham: Springer Nature Switzerland; 2025, p. 30–8.